Electronic Supplementary Information

Environmentally benign pH-responsive cytidine-5'-monophosphate molecule-mediated akaganeite (5'-CMP-β-FeOOH) soft supramolecular hydrogels induced by the puckering of ribose sugar with efficient loading/release capabilities

Anil Kumar* and Priyanka

Department of Chemistry,

Indian Institute of Technology Roorkee,

Roorkee- 247667, Uttarakhand, INDIA.

E-mail: anilkfcy@iitr.ac.in; akmshfcy@gmail.com; Tel.. +91-1332-285799; Fax. +91-1332-273560

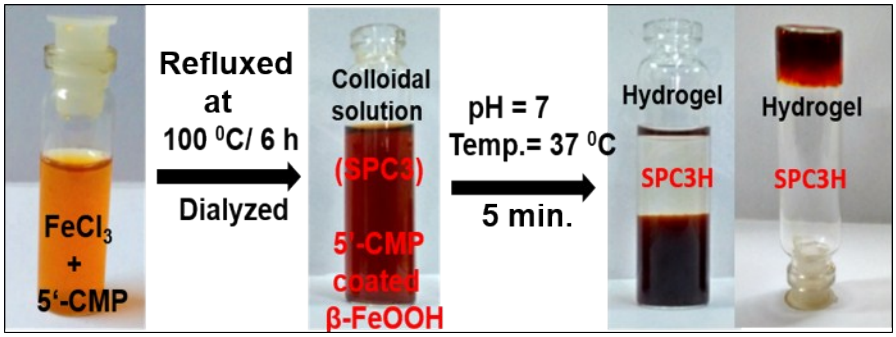

Scheme 1. Presenting the formation of hydrogel (SPC3H) from the dialyzed colloidal solution of 5'-CMP-mediated β-FeOOH (SPC3) in **non-energy intensive process**.

Thermogravimetric analysis (TGA)

The thermal stability of as synthesized solid sample(s) (SPC3, SPC3H and SPB) and 5'-CMP has been examined by performing TGA experiments in the temperature range of 0 to 800 ^{o}C (Fig. S1A and S1B).

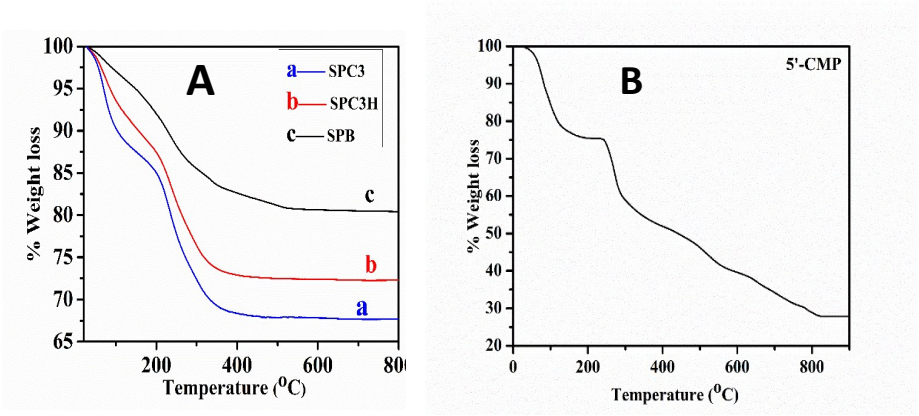

Fig. S1. Thermogravimetric analysis curves **(A):** - SPC3 (a), SPC3H (b), SPB (c); **(B).** 5'-CMP.

A comparison of the TGA curves of these samples clearly shows that the thermal stability arises in the order (% loss in weight, temperature): SPB (18, beyond 510 ^{0}C) > SPC3H (25, beyond 337 ^{0}C) > SPC3 (32, beyond 337 ^{0}C), depicting the bare β-FeOOH to be though the most stable. However, between SPC3 and SPC3H, the latter is found to be more stable. In a control experiment 5'-CMP molecules exhibited >40 % loss in weight upto 300 ^{0}C (Fig. S1B) and decomposes regularly thereafter unlike to that of SPC3H.

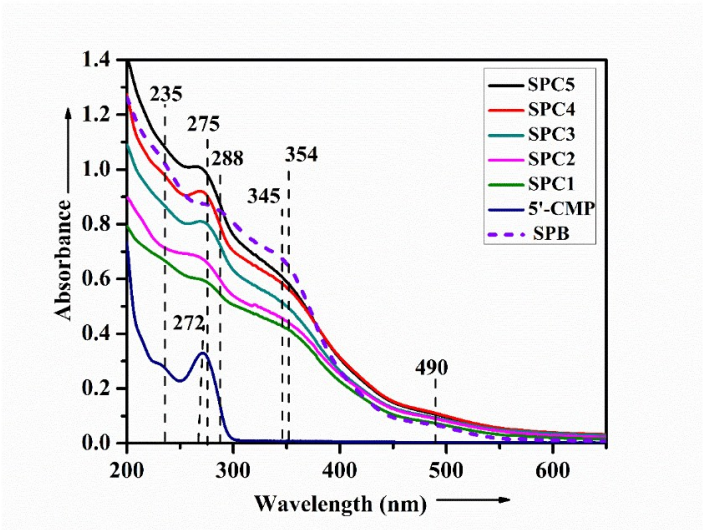

Fig. S2 UV-Vis spectra of SPC (SPC1-SPC5) containing varied [5'-CMP]; absorption spectra of 5'-CMP; ( ) and SPB (-----).

XRD

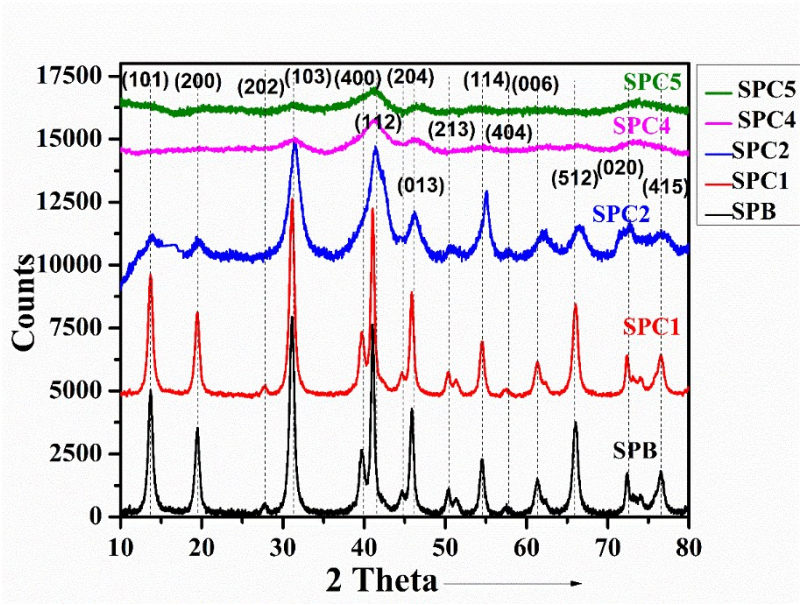

Fig. S3. XRD patterns of colloidal samples at different [5'- CMP] at pH 4.3 along with SPB (β-FeOOH).

Zeta potential

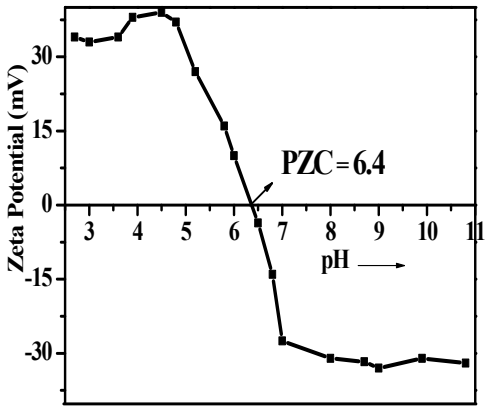

Fig. S4 Zeta potential of SPC3 as a function of pH.

AFM

Pore depth profile for SPC3H

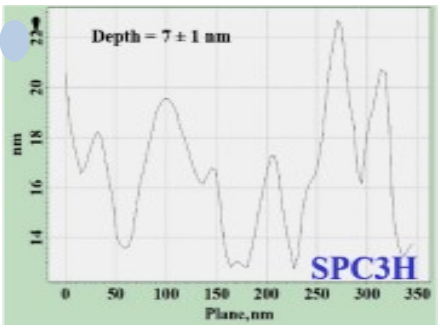

Fig. S5 Pore depth profile of SPC3H.

TEM

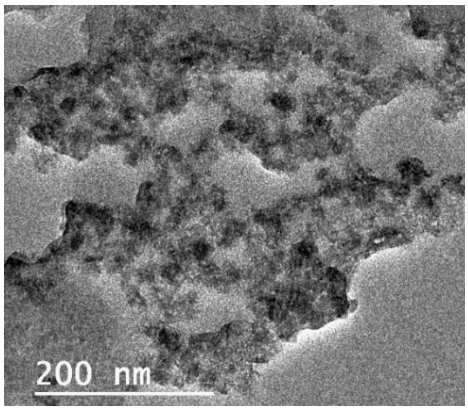

Fig. S6 TEM of SPC3H freeze dried hydrogels.

FESEM

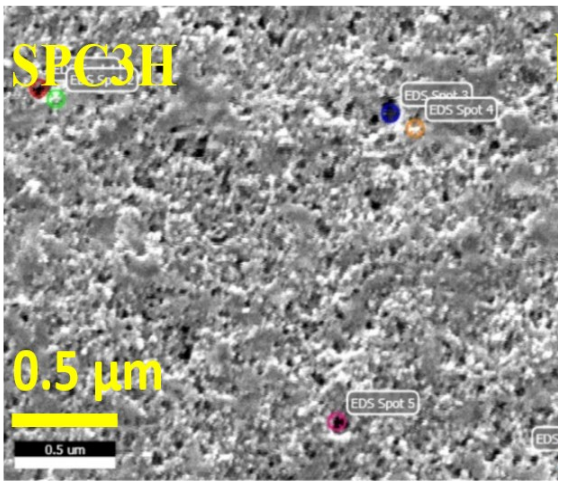

Fig. S7 FESEM images for SPC3H.

Magnetic data

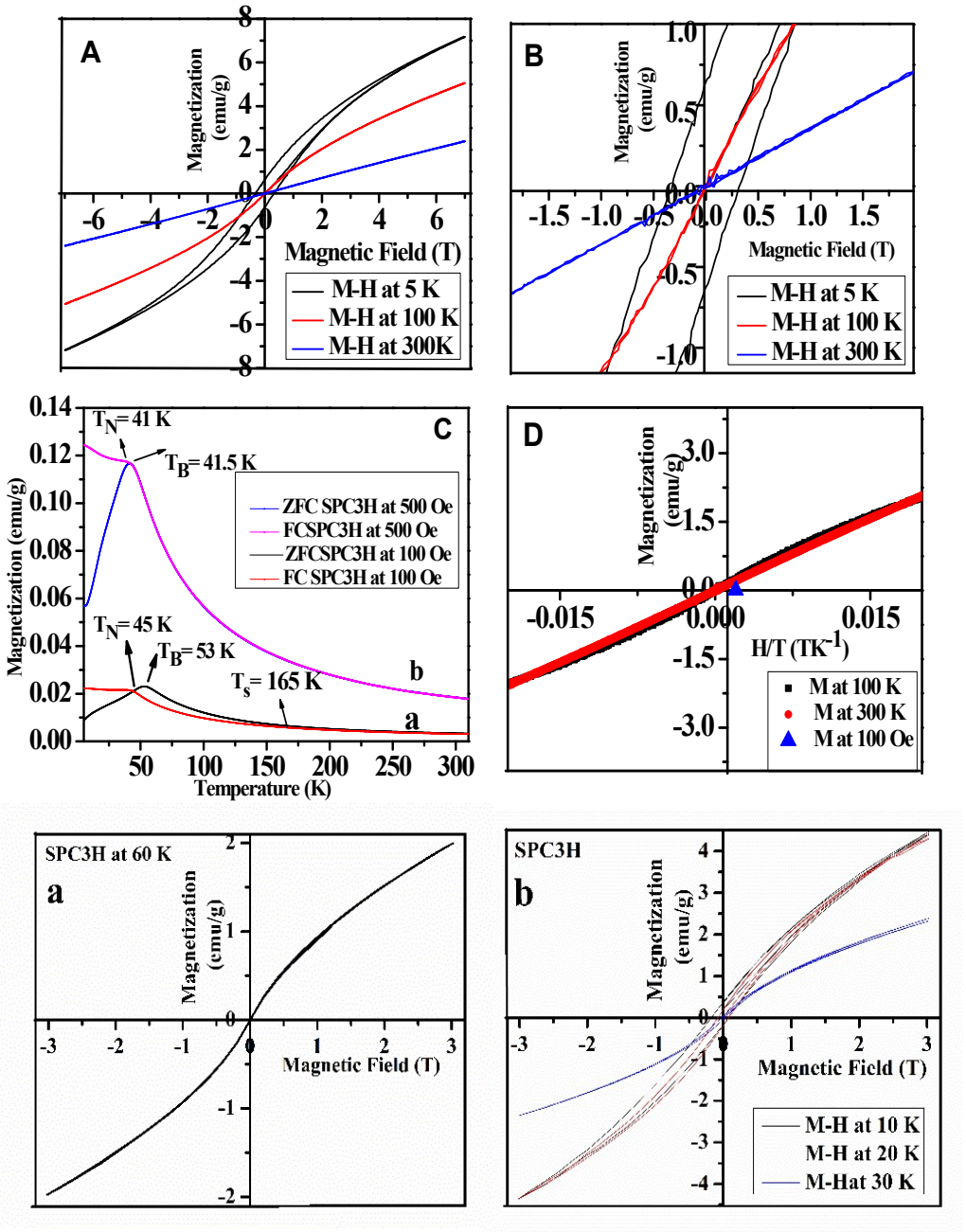

Fig. S8 M-H and FC-ZFC curves of SPC3H: M-H curves at different temperatures (A) and enlarge image of A (B); FC-ZFC curve (C), 100 Oe (curve a), 500 Oe (curve b); M vs H/T curves (D); M-H curves at different temperatures (K): (a) 60; (b) 10, 20 and 30.

Table S1 Magnetization value of SPC3H at different temperatures.

Sample	Magnetization (emu/ g) 5 K	Magnetization (emu/ g) 100 K	Magnetization (emu/ g) 300 K	Coercivity (H_c) (T) 5K
SPC3H	7.17	5.03	2.4	0.3

Raman spectra

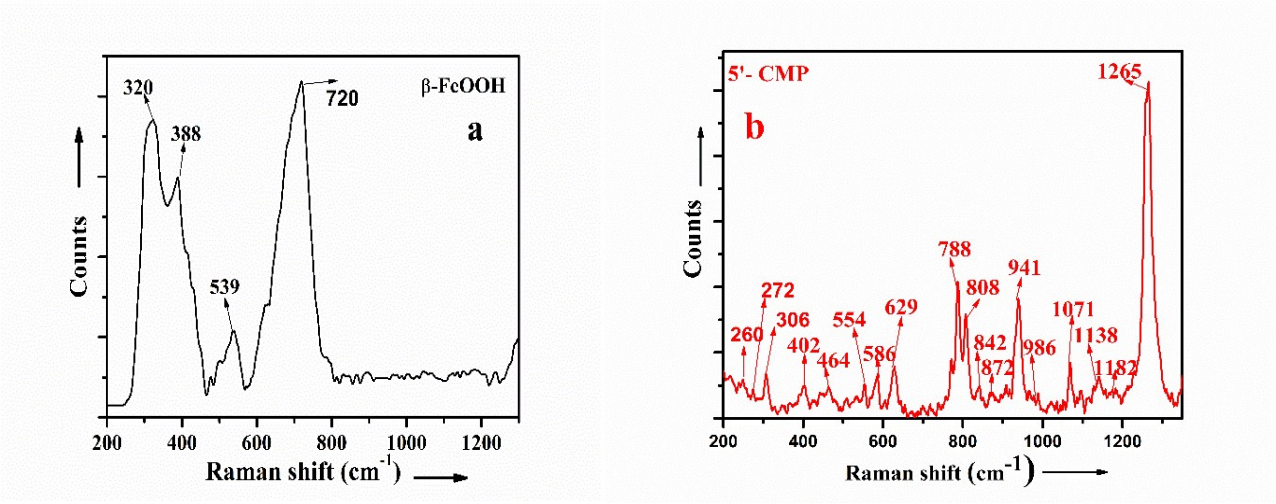

Fig. S9 Raman spectra for (a) Bare β-FeOOH (SPB); (b) bare 5'-CMP at pH 7.

Table S2 Raman spectroscopic data.

Assignment of peaks	Raman peaks for different sample(s) (cm^{-1})			
	Cytidine literature peaks	CMP observed peaks	β-FeOOH observed peaks	SPC3H
Fe-O vib. of octahedral Fe site	-	-	320	322
Fe-O vib. of octahedral Fe site	-	-	388	398
			539, 720	535, 731
RS	408	402	-	-
C+RS	456	464	-	-

δ(C2-N3=C4) and δ(N1-C2-N3)	560	554	-	-
C2=O2 bending	600	586	-	-
δ(N1-C1'-O)	626	629	-	-
Ring breathing	792	788	-	792
P-O str.	818	808	-	-
δ(C2'-C1'-O).	844	842	-	839
RS	870	872	-	-
δ(O3'-C3'H)	944	941	-	948
Out of phase δ(C4-N4H) / PO_3^{2-} str.	986	986	-	978, 994
RS	1074	1071	-	1071
RS	1096	1096		1098
νC4'O-νC4'C3'-δC3'O3'	1117	-	-	1113
δ(C2'C1'H), rNH_2, δ(O1'C1'H)	1138	1138	-	1149
ν(C1'-N1)	1194	1184	-	1182
C+RS	1252	1265	-	1262
δ (C2'-C1')	1291	-	-	1291

*__C__ and __RS__ denote cytosine and ribose sugar, respectively. δ = bending mode, ν = stretching mode, r = rocking mode, br = board.

IR spectroscopy

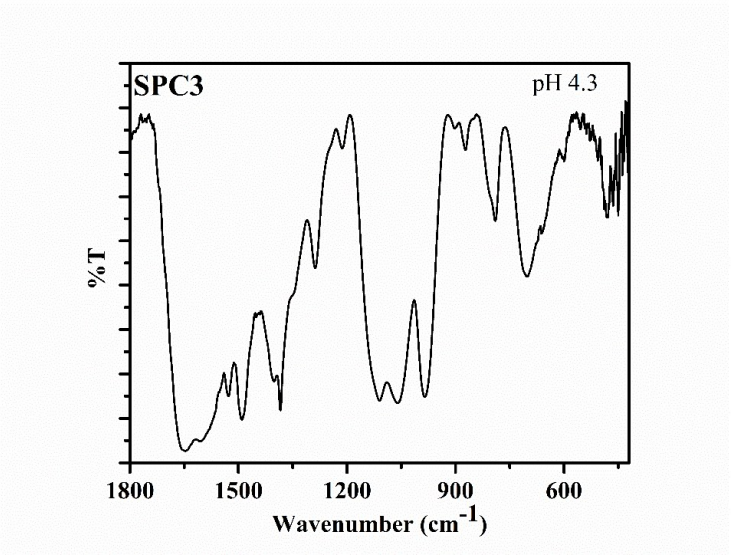

Fig. S10 FTIR of SPC3 at pH 4.3.

Table S3 FTIR spectroscopic data for different samples.

Functional Group/ assignments of peaks	**IR peaks for different sample(s) (cm^{-1})**					
	β-FeOOH literature peaks	**Cytidine literature peaks**	**CMP Observed peaks**	**β-FeOOH Observed peaks**	**SPC3 pH 4.8**	**SPC3H pH 7**
Fe-O-Fe str.	420, 471, 644, 696	-	-	427,480,641, 696		473, 707 (br)
Fe-OH- -Cl deformation	815, 833	-	-	837(s)		diminish
Bending vib. of H_2O	1632	-	-	1632(s)		1632(red. Int.)
Base bending mode		555	546	-	diminish	diminish
δ(N1-C1'-O4')		621	600		600(less int.)	diminish

δ(C2'-Cl'-N1), δ(Nl-Cl'-O4')		630	629		651 (br)	651(br.)
δ (C5-C4-N4)		715	710		707(br)	707 (br) (684-741)
(br)Ring breathing		790	786		790 (br)	790(br, less Int.)
P-O str.		817	817		diminish	diminish
δ(C2'-Cl'-O4')		845	-			852
RS In phase δ (C4'C5'H)		872	873		872(s)	diminish
RS δ (O3'C3'H)		943	945		diminish	diminish
-PO_3^{2-}sym. Str., -NH_2 bending		985	980		984 (br)	984(br, less Int.)
δ(N1-C1'H)		1054	1051		1057(br)	1066 (br)
-PO_3^{2-} deg.		1080	1077		diminish	diminish
(νC4'O-νC4'C3'-δ C3'O3')		1117	1117 (br)		1113(br)	1113(s)(br) new band
δ(C2'C1'H), r(NH2), δ(O1'C1'H)		1154	1147		diminish	diminish
RS δ(C2'O2'H)		1213	1222		1216(less int.)	1216(less Int.)
C+RS		1248	1255		diminish	diminish
C+RS		1294	1295		1286	1286 (less Int.)
RS δ(HC4'O1')		1340	1345		1345	1345(br, less int.)
δ(C4=N3) and (C4-N4)		1505	1496		1491(less int.)	1491(less Int.)

δ(N-H)in plane		1540	1535		1526	diminish
C2=O2 str.		1662	1653		1653 (br)	1653(br) (less int.)

***C** and **RS** denote cytosine and ribose sugar, respectively. δ = bending mode, ν = stretching mode, r = rocking mode, deg. = degeneracy, br = broad, s = sharp, red = reduce.

In control experiments, the spectrum due to 5'-CMP shows various peaks (cm^{-1}) matching to functional groups: 600 (δ(N1-C1'-O)), 629 (δ(C2'-Cl'-N1))/ (δ(Nl-Cl'-O4')), 710 (δ(C5-C4-N4)), 786 (ring breathing), 817 (P-O str.), 872 (δ(C4'-C5'H)), 945 (δ(O3'-C3'H)), 980 (PO_3^{2-} sym. Str. / -NH_2 bending), 1051 (sh, -CH def. with contribution from δ(N1-C1'H)), 1077 (PO_3^{2-} deg.), 1117 (νC4'O-νC4'C3'-δC3'O3'), 1147 (δ(C2'C1'H)/ r(NH2)/ δ(O1'C1'H), 1222 (δ(C2'O2'H)), 1255 (C+RS), 1295 (C+RS), 1345(δ (HC4'O1'), 1496 (δ(C4=N3) and (C4-N4)), 1535(δ(N-H) in plane) and 1657 (C2=O2 str.) matching largely with the literature data (Table S3).

X-ray photoelectron spectroscopy

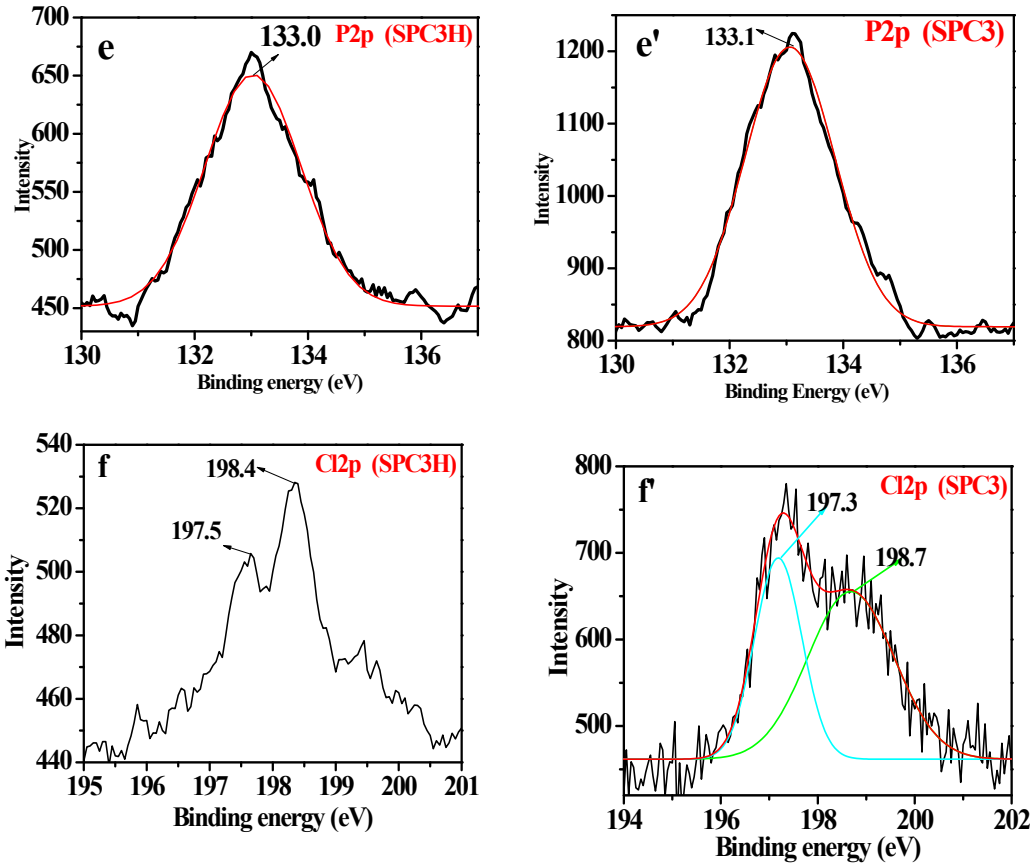

Fig. S11 XPS Spectra of SPC3H and SPC3 for P (e, e') and Cl (f, f') respectively.

Table S4 XPS data for SPC3 and SPC3H.

Elements	**Binding energy (eV) of elements in SPC3H and (intensity/ area)**	**Binding energy (eV) of elements in SPC3 and (intensity/ area)**
Fe	710.09 ((2267.4/885.3) 712.0 (11140.8/2111.9) 718.01 (16914.9/1441.7) 723.54 (900.6/356.6) 725.92 (12011.3, 1752.5)	709.93 (4024.5/1512.0) 711.93 (6435.9/1514.6) 717.8 (1330.1/1468.4) 723.51 (1440.0/492.5) 726.15 (15485.5/2036.2)

O	529.26 (5137/2802.5) 530.5 (2498.8/1853.1) 531.5 (5462.2/2138.4)	528.66 (971.7/832.3) 530.06 (2820.9/1954.1) 531.7 (8291.3/5032.6)
N	398.28 (260.4/201.3) 399.72 (1388.6/585.2) 400.54 (90.7/81.6)	398.07 (201.3/121.3) 399.73 (710.4/206.1) 399.95 (383.9/30.4)
C	284.1 (867.8/565.2) 285.6 (669.5/450.6) 286.8 (1619.4/461.2)	283.4 (3917.5/2673.9) 285.2 (2312.4/1198.4) 287.3 (767.3/425.9)
P	133.0 (199.3/423)	133.0 (386/766)
Cl	197.5 198.4	197.3 (283.3/232.6) 198.7 (433.6/193.3)

Table S5 Rheological data of SPC(s) having different [5'-CMP] at pH 7.

Samples at pH 7.0	**Viscosity (cP)**	**Storage modulus (Pa)**	**Loss modulus (Pa)**	**Yield strain (%)**	**Shear stress (Pa)**	**LVR (%)**
SPC2H	381	38997	1642	5.6	1530	2.5
SPC3H	5557	40169	2307	8.1	1640	4.0
SPC4H	456	38141	2183	2.0	674	1.5

Surface area measurement

The surface area of SPC3H was determined by performing BET measurements by degassing it for 5h at 105 ^{o}C. Its adsorption isotherm curve depicted Type IV behavior (Fig. S16a). Interestingly, DFT analysis of pore size distribution exhibited SPC3H surface to contain both micro- (1.2 nm) as well as mesoporous (4.7 nm) pores (Fig. S16b). The surface area, pore volume and pore width data obtained from these measurements are compiled in Table S7.

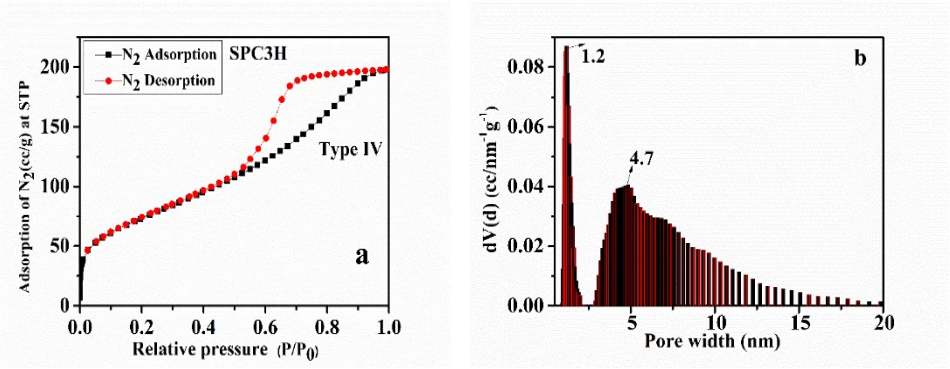

Fig. S12 (a) Adsorption isotherm of SPC3H; (b) pore size distribution by using DFT calculation.

Table S6 BET data of SPC3H at pH 7.0.

Sample	Surface area (m^2/g)	Pore width (nm)	Total pore volume (cc/g)
SPC3H	269	1.2 and 4.7	0.31

Release of MB at pH 5.5

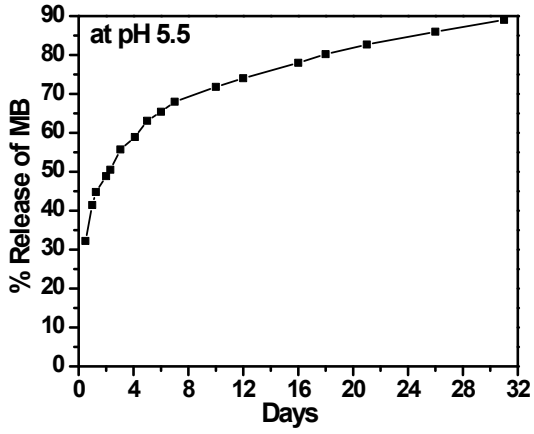

Fig. S13 Release of MB at pH 5.5.

Sensing of alcohol

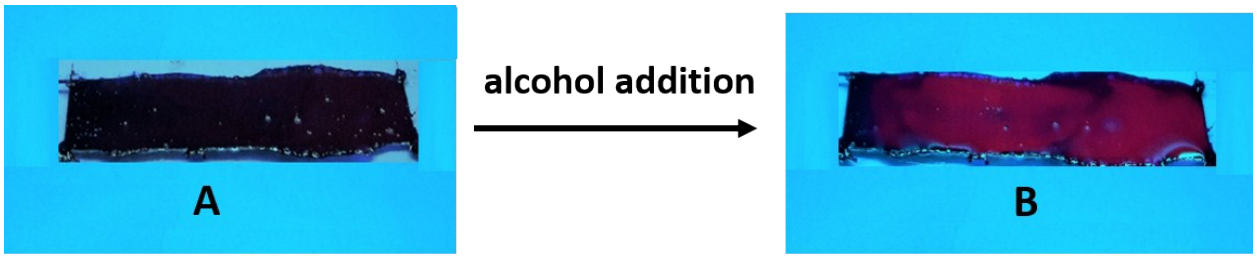

Fig. S14 (A) SPC3H gel and NB before addition of alcohol; (B) SPC3H gel and NB after addition of alcohol.

Adsorption and release of MB on FD gel at pH 7.

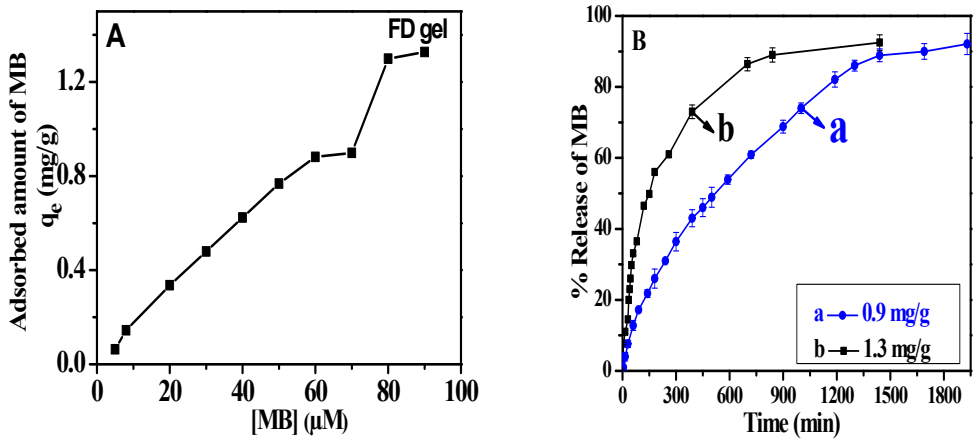

Fig. S15 (A) Adsorption isotherm of MB on FD gel; (B) Release profile of MB for: 5.5 μM (curve a); 8 μM (curve b) adsorbed on FD gel at pH 7.

In case of FD hydrogels, the adsorbed amount of MB as a function of its initial concentration is presented in Fig. S15A. The adsorption isotherm for MB exhibits it to be of Type IV. At its lower concentrations (60 μM) it matched to Type I isotherm, whereas at its higher concentrations, *i.e.* beyond >60 μM, it either might be showing a secondary adsorption on the surface of hydrogels or starts entering into the available pores. The amount of adsorbed MB corresponding to the first and second plateau comes out to be 5.5 μM (0.9 mg/g) and 8.0 μM (1.3 mg/g) (Fig. S15A) and its release profile for the different amount of adsorbed MB are shown in Fig. S15B. From these curves it is apparent that the release for higher [MB] was almost linear up to 35%, thereafter it slows down and attained the plateau value after about 12 h. Whereas, the release becomes relatively much slower for the lower amount of the adsorbed dye taking about 33 h for 91% release similar to that observed for the soft hydrogel.

Cell viability

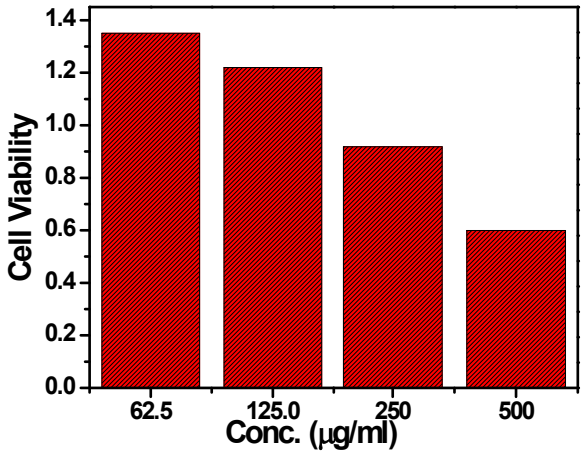

Fig. S16 Cell viability bar diagram of different [SPC3H] on 293T human embryonic kidney cell.

Rheology measurements at pH 5.8

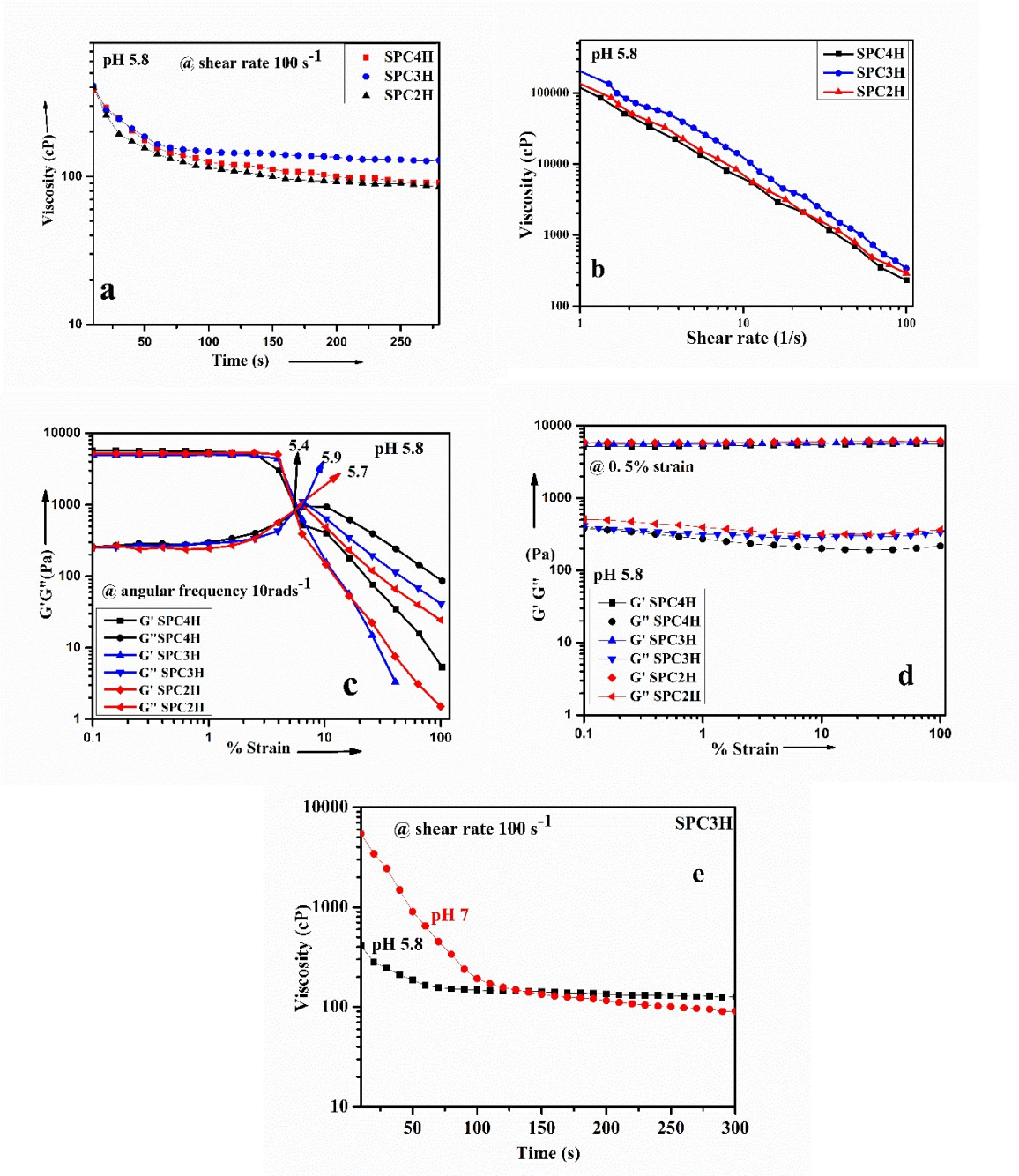

Fig. S17 Viscosity of various hydrogels samples at fixed shear rate 100 s^{-1} (a); viscosity profile for the shear sweep of hydrogels samples (b); viscoelastic behavior of gel: (B) amplitude sweep oh hydrogels samples at fixed angular frequency 10 rad s^{-1}(c); frequency sweep curve for hydrogels at fixed strain 0.5% (d); viscosity of SPC3H at pH 5.8 and 7.0 (e).

In order to optimize the viscoelastic behavior of hydrogels their rheological behavior was investigated as a function of [5'- CMP] ranging from 1.5 to 3.5 mM at pH 5.8 and these samples have been abbreviated as: [5'- CMP] (mM) (abbreviation) - 1.5 (SPC2H); 2.5 (SPC3H) and 3.5 (SPC4H) (Fig. S17; Table S7). The storage modulus (G') was always higher than that of the loss modulus (G'') (Table S7). Whereas, the viscosity follows the order: SPC2H < SPC3H > SPC4H (Fig. S17a), indicating that the viscosity initially

increases with increasing the [5'-CMP] and, thereafter it is decreased. The stability of hydrogel was further examined by monitoring the viscosity as a function of shear rate (Fig. S17b). For all the samples it was found to decrease with increasing the shear rate, indicating the formation of hydrogels in all these samples. From rheological data it is observed that the best viscoelastic properties correspond to SPC3H suggesting that 2.5 mM [5'- CMP] produced the most stable hydrogel.

Table S7 Rheological data for different hydrogels samples at pH 5.8.

Samples at pH 5.8	**Viscosity (cP)**	**Storage modulus G' (Pa)**	**Loss modulus G'' (Pa)**	**Cross over (%strain)**	**Ratio of G'/ G''**
SPC4H (3.5 mM)	384	5696	292	5.7	19.5
SPC3H (2.5 mM)	410	4932	242	5.9	20.4
SPC2H (1.5 mM)	390	5225	250	5.4	20.9